Computation of exciton binding energies in exciton condensation

Anna O. Schouten, LeeAnn M. Sager-Smith,* and David A. Mazziotti†
Department of Chemistry and The James Franck Institute, The University of Chicago, Chicago, Illinois 60637, USA

(Received 5 June 2023; revised 31 May 2024; accepted 17 June 2024; published 2 July 2024)

Exciton binding energies are fundamental to understanding excitonic materials, especially those with the potential for ground-state exciton condensation. However, these energies are typically defined with significant limitations in their consideration of electron correlation. Here we present a variational theory for computing exciton binding energies in ground-state exciton condensates in which we define the binding as the energy difference between fully correlated many-electron systems with M and $M-1$ excitons, respectively. The $(M-1)$ system is obtained by adding a constraint to the ground-state energy minimization that removes an exciton while allowing all other electronic degrees of freedom to relax. We perform the energy minimizations with variational calculations of the two-electron reduced density matrix (2-RDM) in which the additional constraint is treated along with the N-representability conditions—necessary constraints for the 2-RDM to represent an N-electron system—by semidefinite programming. We demonstrate the theory first in the Lipkin model and then in several stacked organic and inorganic systems that exhibit the beginnings of exciton condensation. We find that in the Lipkin model the traditional exciton binding model overbinds relative to the constrained approach. This has significant implications for theoretical characterizations of exciton condensates which rely on exciton binding energy to make predictions regarding condensate stability and critical temperatures. This correlated approach to defining and computing exciton binding energies may therefore have important applications for understanding the relationship between binding and condensation, especially for the BCS-BEC crossover.

DOI: 10.1103/PhysRevB.110.035110

I. INTRODUCTION

Excitons are bosonic quasiparticles formed from bound electron-hole pairs. Because excitons are bosonic in nature, they can undergo condensation into a single quantum state, analogous to Cooper-pair condensation in superconductors [1–3]. Such condensation typically occurs in strongly correlated systems (systems which cannot be accurately represented by a single antisymmetrized orbital-product wave function) and results from correlation exhibited as long-range order [4]. Condensation of excitons, or exciton condensation, was initially postulated in the mid-20th century and has received considerable attention, particularly in recent years, for its potential for superfluid transport of energy [3,5–16]. Exciton condensates are also sometimes known as excitonic insulators, which form at low temperatures when the magnitude of the exciton binding energy exceeds that of the noninteracting energy gap, leading to the opening of a many-body condensate gap [17–19]. Exciton binding energy is thus crucial to understanding the formation of exciton condensates and influences properties of condensation such as exciton density and critical temperature.

Exciton binding energy is also important as an indicator of excitonic stability in semiconductors and similar systems in which excitons function as charge and energy carriers. Like binding energy in a hydrogen atom, exciton binding energy can be simply defined as the energy binding the electron and hole; however, while physically straightforward, this quantity is difficult to calculate. For Wannier-Mott excitons, Wannier used the similarity to the hydrogen atom to develop a hydrogenlike model to approximate exciton binding energy, and other approximate methods have subsequently been developed based on this model [20–22]. For tight-binding excitons, exciton binding energy is instead typically calculated from experimental spectra as the energy difference between the transport gap and the optical gap [23,24]. Computational methods using the Bethe-Salpeter equation (BSE) and many-body perturbation theory determine this through the energy difference between a quasiparticle—or single-particle—gap and the excitation energy [25–27]. Theoretical predictions of the onset of exciton condensation are frequently made using these methods to calculate exciton binding energies and energy gaps [28–30]. Although these methods provide valuable descriptions of exciton binding for many systems and can even provide insight into the onset of exciton condensation for some cases, they rely on mean-field references or simplified models that neglect strong correlation. Thus, for strongly correlated systems, interactions may not be accurately treated. In the case of exciton condensation, a single-particle perspective like this also ignores the consideration of many-particle interactions, which are important for understanding condensation, particularly given the many-body nature of the condensate gap [31].

In this paper we introduce a method for calculating exciton binding energy that is rooted in the correlated nature of excitons and exciton condensation. We directly connect binding energy to exciton condensation by defining binding energy as the energy required to remove an exciton from an exciton condensate. This represents an integrated exciton chemical potential, i.e., the finite-energy difference due to a change in the

*Present address: Department of Chemistry and Physics, Saint Mary's College, Notre Dame, Indiana 46556, USA.
†Contact author: damazz@uchicago.edu

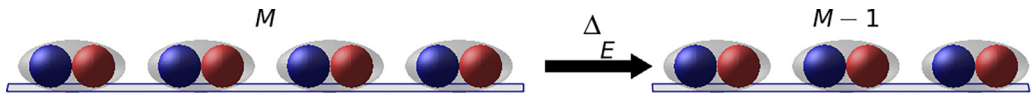

FIG. 1. A schematic representing the binding energy. The binding energy is defined as the difference between the energy of the condensate with M excitons and that of the system with $M-1$ excitons.

number of particles. In exciton condensates, the exciton chemical potential is used to predict both the onset of condensation and exciton binding energy, the magnitude of which is associated with the value of the exciton chemical potential [32–37]. For systems in which the chemical potential can be controlled through the tuning of carrier densities, exciton binding energies can be experimentally obtained from the exciton chemical potential. This accounts for the influence of condensation on exciton binding due to excitonic interactions. The definition of exciton binding energy we introduce is conceptually similar, potentially allowing for insights into the effect of condensation on exciton binding. Using a computational signature for exciton condensation [38,39], we present a method for calculating this energy and demonstrate this method for the exactly solvable but highly correlated Lipkin model [40]. Results from the Lipkin model display divergence of the traditional exciton binding picture from our method as interaction increases, with the traditional model overbinding relative to our method. We then apply this method to several molecular systems [41,42]. The method is based on variational 2-RDM theory, previously developed by one of the authors and applied to a variety of strongly correlated systems [43–49]. We observe binding energies on the same orders of magnitudes as reported exciton binding energies in similar systems. Consistent with other reports, the binding energies are impacted by structural factors influencing exciton delocalization and size, such as interlayer distance and number of layers.

II. THEORY

Like Bose-Einstein condensation (BEC) of liquid helium and superconductivity resulting from condensation of Cooper pairs, exciton condensation is associated with long-range order. This long-range order is identifiable from signatures in the relevant reduced density matrices (RDMs) [4,50,51]. Excitons are bound particle-hole pairs, so there is a signature for exciton condensation in the particle-hole RDM:

$$ {}^2G^{i,j}_{k,l} = \langle\psi|\hat{a}^\dagger_i\hat{a}_j\hat{a}^\dagger_l\hat{a}_k|\psi\rangle. \tag{1}$$

The particle-hole RDM is related to the two-electron RDM (2-RDM) by a linear mapping as follows:

$$ {}^2G^{i,j}_{k,l} = {}^1I^j_l\,{}^1D^i_k - {}^2D^{i,l}_{k,j}, \tag{2}$$

where ${}^1I$ is the identity matrix, ${}^1D$ is the one-electron RDM, and ${}^2D$ is the 2-RDM:

$$ {}^2D^{i,l}_{k,j} = \langle\psi|\hat{a}^\dagger_i\hat{a}^\dagger_l\hat{a}_j\hat{a}_k|\psi\rangle. \tag{3}$$

The signature for exciton condensation is obtained from the eigenvalues of the particle-hole RDM [38,39]:

$$ {}^2Gv_i = \lambda_i v_i. \tag{4}$$

Because of the Pauli exclusion principle, in an uncorrelated system, all but one of the eigenvalues of the particle-hole RDM are bound by 1. (The first eigenvalue corresponds to ground-state-to-ground-state projection, essentially an electron counting operator, and is always larger than 1.) When exciton condensation occurs, however, there is a second eigenvalue greater than 1. This eigenvalue is therefore a definitive signature for long-range order associated with exciton condensation since in the absence of condensation it cannot exceed 1.

As Penrose and Onsager [4] showed for BEC—for which they demonstrated that the signature of BEC is an eigenvalue greater than 1 in the one-boson RDM—the size of the eigenvalue indicates the number of particles in a single boson orbital, or the number of bosons in the condensate state. When Yang [50] and Sasaki [51] showed that an eigenvalue greater than 1 in the 2-RDM represents electron-electron condensation, they demonstrated that the size of the eigenvalue of the 2-RDM represents the occupation of a geminal, or two-particle wave function. By analogy, a similar interpretation of the size of the eigenvalue of the particle-hole RDM applies to excitons [38,39]. Thus, the magnitude of the large eigenvalue indicates the occupation of a particle-hole wave function or the size of the exciton condensate; e.g., if the eigenvalue equals 3, there are three excitons in the exciton condensate. Note, however, that the eigenvalue need not be an integer because any value greater than 1 results from more than one exciton occupying a single particle-hole orbital or condensation of excitons such that, for instance, an eigenvalue of magnitude 1.5 indicates the beginnings of exciton condensation. The beginnings of exciton condensation represent the start of the long-range order associated with such condensation, which is a critical seed necessary for exciton condensation to occur on the macroscopic scale.

We define the exciton binding energy as the energy required to remove one exciton from an exciton condensate, i.e., the energy difference between an exciton condensate of M excitons and the same condensate with $M-1$ excitons. A schematic representation of this is shown in Fig. 1, illustrating the energy change when one exciton is removed from the system. In the molecular framework, this definition of the exciton binding energy represents the particle fluctuation energy—the chemical potential—which is associated with the exciton binding energy [32–37]. In contrast to methods that calculate a single-particle binding energy, this definition corresponds to a many-body exciton condensate binding energy that accounts for exciton binding in the condensate.

The binding energy is calculated as the energy difference of the ground state with an exciton condensate of size M ($E^*_{\rm gs}$) and a nonequilibrium ground state for which a constraint is placed on the large eigenvalue signature to reduce the same condensate to size $M-1$ ($E^*_{\rm noneq}$), such that the exciton binding energy is equal to the energy difference:

$$ \Delta_E = E^*_{\rm noneq} - E^*_{\rm gs}. \tag{5}$$

The energy of the ground state associated with the exciton condensate of M excitons is expressible as

$$E^*_{\mathrm{gs}} = \min_{{}^2D \in {}^2\mathbb{P}_N} E[{}^2D], \tag{6}$$

where ${}^2\mathbb{P}_N$ is the set of N-representable or approximately N-representable 2-RDMs. The 2-RDM is N-representable if and only if it is representable by at least one N-electron density matrix [52]. The set of density matrices ${}^2\mathbb{P}_N$ can be selected from a hierarchy of N-representability conditions in the form of linear matrix inequalities, i.e., positive semidefinite constraints [53,54]. Hence, the minimization problem is expressible as a semidefinite program [43–45,55–57]. The Appendix summarizes the approximate set of N-representability constraints known as the 2-positivity conditions. An additional constraint is added to calculate the nonequilibrium ground state energy constraining the large eigenvalue signature of exciton condensation. As the first large eigenvalue corresponding to ground-state-to-ground-state projection is unrelated to exciton condensation, this eigenvalue is ignored, and the signature for exciton condensation is the second large (greater than one) eigenvalue in the particle-hole RDM. The magnitude of the large eigenvalue determines the value of M that defines the exciton condensate of M excitons, so a constraint is placed on the eigenvector corresponding to this eigenvalue in the ground state calculation to remove up to one exciton from the eigenvalue. The energy of the nonequilibrium ground state associated with the exciton condensate of c excitons is therefore expressed as

$$E^*_{\mathrm{noneq}} = \min_{{}^2D \in {}^2\mathbb{P}_N} E[{}^2D] \tag{7}$$

such that

$$v^T\, {}^2G[{}^2D]\, v = c, \tag{8}$$

where c is the value of the constrained eigenvalue and v is the eigenvector associated with the large eigenvalue mode. Effectively, this calculates a new ground state energy, but for a state with an exciton removed from the original ground state. Thus, while our system will be higher in energy because the constraint forces the system away from the original ground state, the resulting energy is still relaxed to a minimum energy for the constrained state. Physically, the energy difference between the ground and constrained states is the energy associated with removing the exciton from the condensate or the binding energy of an exciton in the condensate. The constraint does not specify what happens to the exciton after removal, so the particle and hole are free to separate. Additionally, it is important to note that because the new energy corresponds to a relaxed ground state, constraining the original exciton condensate does not preclude formation of a new exciton condensate, discernible as a different large eigenvalue. The constraint applies only to the mode corresponding to the specified eigenvector, so it is possible to observe a new signature for exciton condensation if such a phase exists in the lowest energy state meeting the conditions of the constraint. However, it is not necessary to constrain every possible large eigenvalue, as the physical interpretation of this would be the removal of multiple excitons, each from a different mode, and would confuse the interpretation of the binding energy.

III. APPLICATIONS

A. Lipkin model

We use the correlated method to calculate exciton binding energies for the Lipkin model [40] and compare the results to the traditional picture of exciton binding. The Lipkin model is an exactly solvable model of electrons confined to a two-level system with scattering terms which excite and deexcite pairs of electrons between the upper and lower levels. The Hamiltonian is given by

$$\hat{H} = \frac{\epsilon}{2} \sum_p \hat{a}^\dagger_{1,p} \hat{a}_{1,p} - \hat{a}^\dagger_{-1,p} \hat{a}_{-1,p} \tag{9}$$

$$+ \frac{V}{2} \sum_{p,q} \hat{a}^\dagger_{1,p} \hat{a}^\dagger_{1,q} \hat{a}_{-1,q} \hat{a}_{-1,p} + \hat{a}^\dagger_{-1,p} \hat{a}^\dagger_{-1,q} \hat{a}_{1,q} \hat{a}_{1,p}, \tag{10}$$

where $\hat{a}_{1,p}$ ($\hat{a}^\dagger_{-1,p}$) annihilates (creates) a particle in the upper (lower) level of site p, $\epsilon/2$ is the energy gap of the two levels, and $V/2$ is the interaction strength between pairs of scattered particles. When $V = 0$, the system is completely noninteracting, but the interaction in the system increases with V, leading to a macroscopic large eigenvalue in the particle-hole RDM for strongly interacting systems with a large particle number N [58].

Exciton binding energies and λ_G are shown for the Lipkin model with $\epsilon = 1$ and $N = 10$ in Fig. 2(a). Figure 2(a) shows the growth of the magnitude of λ_G (blue) with the interaction strength for $N = 10$. Note that λ_G approaches an upper bound determined by N in the strongly interacting regime. Binding energies are calculated for the traditional binding energy as the difference between the noninteracting gap ($V = 0$) and the interacting gap ($V > 0$) obtained from exact diagonalization of the Hamiltonian according to

$$E_B = \frac{1}{N}[(E_{G,\mathrm{I}} - E_{N,\mathrm{I}}) - (E_{G,\mathrm{NI}} - E_{N,\mathrm{NI}})], \tag{11}$$

where E_G is the ground state energy of either the interacting (I) or noninteracting (NI) model, E_N is the excitation energy, and $1/N$ is the normalization. The Lipkin model is also solved using variational 2-RDM theory (see the Appendix), and binding energies are calculated by constraining λ_G as described in Sec. II. Constraints for calculating the binding energies according to the constrained eigenvalue definition are applied in two ways: (1) the large eigenvalue is constrained by 1, i.e., removal of a single exciton, and (2) the eigenvalue is fully constrained to 1, then scaled by the eigenvalue difference, i.e., the energy to destroy the condensate normalized by the size of the condensate. Note that binding energies for the constrained method can be obtained for the model only when $\lambda_G > 1$. It is important to compare the two constraints for calculating binding energy from the constrained eigenvalue definition—the energy to remove a single exciton versus a normalized condensate constraint—because in systems which exhibit only the beginnings of exciton condensation, as in the section below, while λ_G is large enough to indicate the beginnings of exciton condensation, the magnitude is too small to remove one whole exciton, but by constraining the eigenvalue to 1 and normalizing by the eigenvalue difference, we obtain

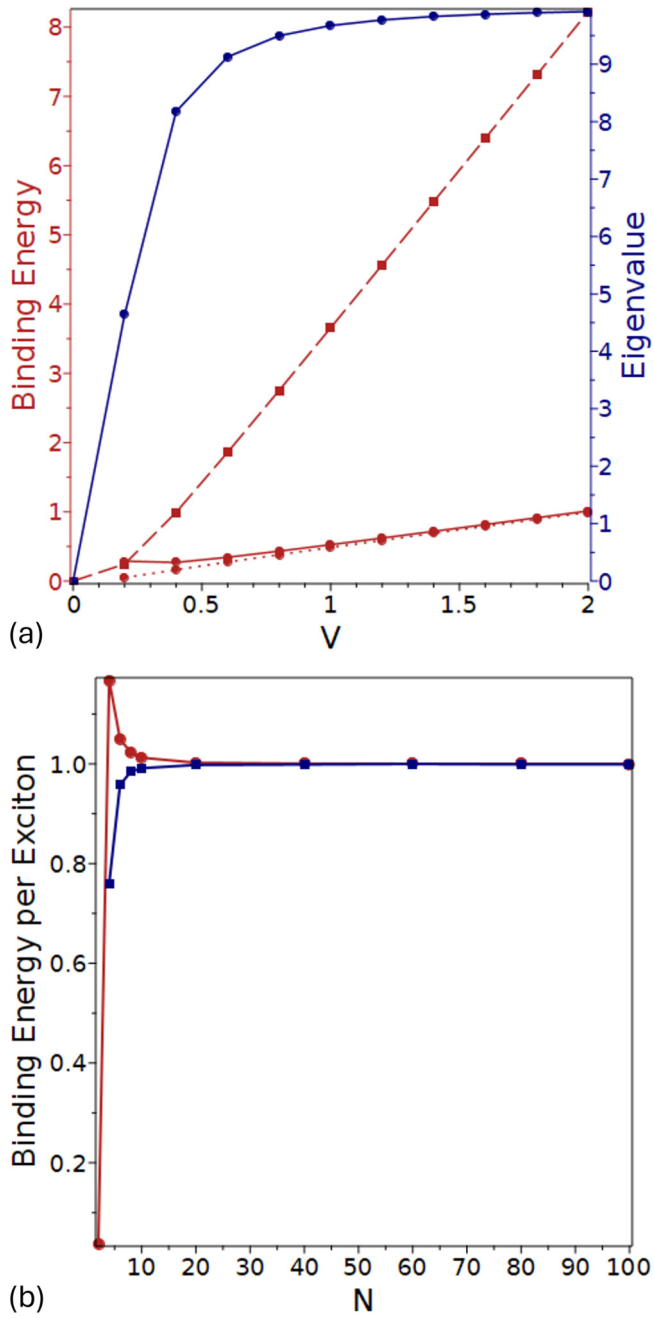

FIG. 2. (a) Exciton binding energies (red) and λ_G (blue) calculated for the Lipkin model with $\epsilon = 1$, $N = 10$, and variable V using the traditional definition (dashed line with squares), the correlated method with the eigenvalue constrained by one exciton (dotted line with circles), and the correlated method with the eigenvalue constrained to 1, then scaled by the eigenvalue difference (solid line with circles). (b) Exciton binding energies for the Lipkin model with $\epsilon = 1$, $V = 2.0$, and variable N for the correlated method with the eigenvalue constrained by 1 (blue) and the eigenvalue constrained to 1 and scaled by the eigenvalue difference (red).

an estimate of the binding energy. As shown in Fig. 2(a), this way of estimating the binding of a single exciton by a normalized condensate constraint converges with the binding energy calculated by constraining a single exciton in the strongly interacting limit.

The results of the Lipkin model allow us to make comparisons between the traditional definition of binding energy and the constrained definition and infer the relationship of the two binding energies. In the weakly interacting regime ($V = 0.2$), the traditional binding energy and the constrained binding energy are in agreement [Fig. 2(a)]; however, while binding energies produced from both methods then increase approximately linearly with interaction strength, the traditional binding energy increases much more rapidly, demonstrating divergence of the two definitions with strong interaction. This leads to traditional binding energies that approach an order of magnitude larger than the noninteracting excitation energy in the extreme interaction limit.

By increasing the value of N, we observe the behavior of the system as it approaches the thermodynamic limit. Figure 2(b) shows the binding energy per exciton for the constrained method in the strongly interacting regime ($V = 2.0$) with increasing N, calculated both by the removal of a single exciton and by the normalized condensate constraint estimate. In this regime λ_G approaches the upper limit of condensation for N. The binding energy quickly converges as the number of particles increases to reach a constant value on the order of the noninteracting excitation energy, indicating exciton binding and condensation results in a gap of magnitude similar to the noninteracting excitation energy. The convergence of the binding energy with increasing N seems intuitive, as one might expect that the size of the condensate would impact the strength of binding significantly in small systems, but in large systems a "bulk material" limit of binding should be reached where the size has less impact on the strength of the binding energy. Note that for low particle numbers there is a difference between the single-exciton constraint and normalized condensate constraint binding energies. This is due to slight overestimation of the binding energy by the normalized condensate constraint for low numbers of particles which approaches the single-exciton energy as N increases. Additionally, for $N = 2$, $1 < \lambda_G < 2$ due to the small number of particles in the system, so only the normalized condensate constrained binding energy can be calculated. However, despite the slight overestimation these results suggest that the normalized condensate constraint provides a reasonable estimate of the true binding energy per exciton, which can provide insight into the nature of exciton binding even in a small system.

B. Molecular systems

We apply our method of calculating the binding energy of several molecular systems in which we previously observed the beginnings of exciton condensation via the large eigenvalue: van der Waals stacks of benzene [41], Bechgaard saltlike tetrathiafulvalene (TTF) stacks, and the molecular analog of the amorphous polymer nickel tetrathiafulvalene-tetrathiolate (NiTTFtt) [42]. The molecular structures of dimers of the three materials are shown in Fig. 3. We demonstrate the influence of structural factors on binding energy, including molecular composition, interlayer separation distance, and system size. All calculations are performed using the variational 2-RDM method as described in Sec. II and the Appendix. The method is implemented as an extension of the variational 2-RDM method in the Quantum Chemistry Toolbox in Maple [59,60]. The 6-31g basis set is used for all

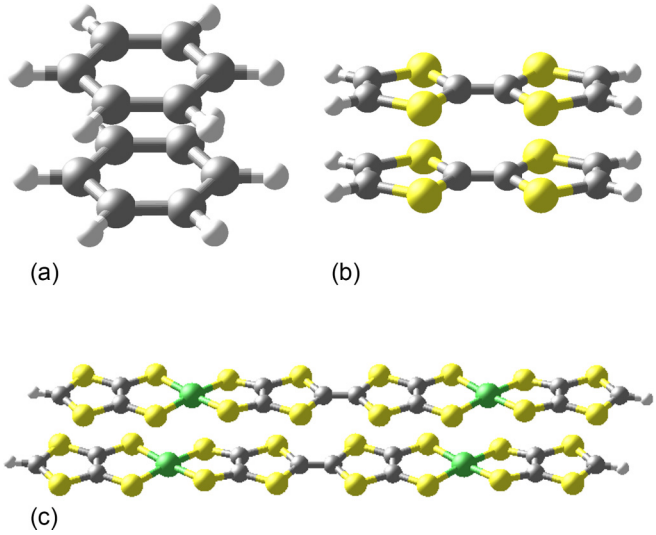

FIG. 3. (a) Benzene dimer, (b) TTF dimer, and (c) NiTTFtt dimer.

calculations. All bilayer calculations employ a [12,12] active space, and the active space grows with system size for greater numbers of layers, i.e., [18,18] for three layers, [24,24] for four layers, etc.

In a macroscopic system, the large eigenvalue signature of exciton condensation would be expected to have values much larger than 1, so that $M \geqslant 2$ and $M - 1 \geqslant 1$. The true binding energy is therefore the energy difference if one whole exciton is removed, so in a system where the eigenvalue is greater than 2, this would be the energy for a constraint of size 1. However, in the molecular systems we explore, the signature indicates only the beginnings of exciton condensation; thus, the eigenvalue is greater than 1 but is not greater than 2. Consequently, we calculate the binding energy by constraining the whole condensate and normalizing the energy difference to one exciton by scaling the energy by the magnitude of the eigenvalue constraint. From the Lipkin model calculations we observe that while this overestimates the binding energy in the low-interaction and small-N limit, it converges with the true binding energy, making it an appropriate estimate of the binding energy that can be used to interpret trends in binding energy.

Figure 4 shows plots of the interlayer distance versus the large eigenvalue (blue, right axis) and the binding energy (red, left axis) for bilayers of benzene, TTF, and molecular NiTTFtt. One notable feature of the plots is the difference in the magnitudes of binding energies for the three materials. TTF has the largest binding energies, with binding energies ranging from about 0.5 to 5 eV. Binding energies for benzene are only slightly lower, with binding energies ranging from about 0.2 to 0.9 eV. NiTTFtt has the lowest binding energies, with energies ranging from about 15 to 100 meV.

Exciton binding energies reported for thiophenes of increasing length are on the order of several eV, like binding energies we observe for TTF, indicating the binding energies for TTF are reasonable [61]. The magnitudes of the benzene dimer binding energies are also consistent with reported exciton binding energies for organic molecules, including benzene and other acenes, which can range from ∼0.5 to 1.5 eV and are reported to be larger for small molecules [62–65]. The smaller magnitudes of the binding energies for NiTTFtt also appear to be reasonable with respect to binding energies for other inorganic materials. The large range of exciton binding energies for these three materials are not dissimilar to ranges reported in the literature for a variety of inorganic layered materials which range from several meV to thousands of meV (several eV). The large differences in binding energies between materials have been attributed to differences in the delocalization of the excitons [66]. We do not compare exact values of binding energies to traditional methods because the constrained definition of binding energy is based on condensation rather than single-particle binding, so the two definitions are not mathematically equivalent, as demonstrated for the Lipkin model. However, we observe that the trends in binding energy, which are important for predicting exciton condensation, are consistent between definitions.

Interlayer excitons, excitons formed from electrons and holes contained in separate molecular layers or layers of a material, have increased stability because the spatial separation helps prevent recombination, extending the lifetime of the exciton [67]. As such, layered structures with interlayer

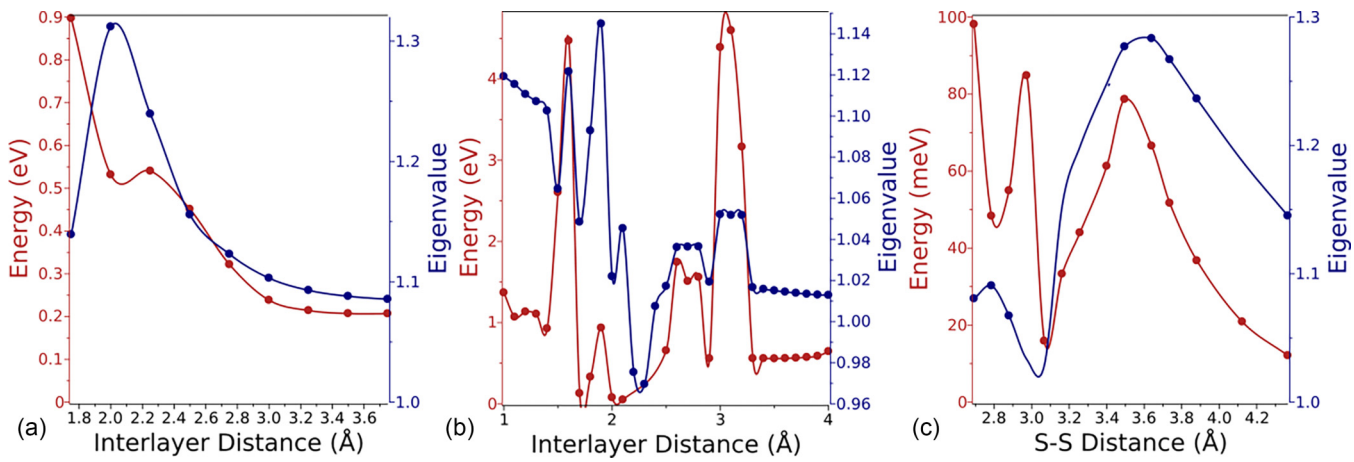

FIG. 4. Exciton binding energy and signature of condensation as a function of interlayer distance for double layers of (a) benzene, (b) TTF, and (c) NiTTFtt. Binding energy is shown in red (left axis), and the eigenvalue is shown in blue (right axis).

excitons appear to be good candidates for exciton condensation. Indeed, the molecular systems in which we observe the signature for exciton condensation are layered systems, and we observe that in molecular layers, the interlayer distance influences the potential for exciton condensation indicated by the large eigenvalue. The plots in Fig. 4 display a pattern with respect to the relationship between the binding energy and interlayer or sulfur-sulfur (S-S) distance for all three materials. The S-S distance is similar to interlayer distance but accounts for a face-to-face shift between layers that mimics the amorphous geometry of NiTTFtt. Although the binding energies are generally higher with larger eigenvalues, indicating that greater potential for exciton condensation occurs with larger possible binding energies, at short interlayer or S-S distances, the binding energy is increased relative to bilayers with similar potential for exciton condensation and larger interlayer or S-S distances. This trend suggests these systems contain interlayer excitons which are more tightly bound at closer interlayer distances.

For TTF, we observe two important peak regions: the small interlayer distance region (interlayer distance of less than 2 Å) and a region with interlayer distance of around 3 Å. Where the eigenvalue is only slightly greater than 1 ($\lesssim$1.05), it is difficult to interpret the binding energy because the degree of condensation is so small, so we focus on regions where $\lambda_G \gtrsim 1.05$. At lower interlayer distance, the magnitudes of both the eigenvalues and the binding energy are influenced by close interlayer interactions. Note that within this region the interlayer distance is near or slightly below the average van der Waals radii of sulfur and carbon, resulting in more tightly bound states and leading to large peaks in binding energy, like the peak around 1.6 Å interlayer distance. Dips in the binding energy in this region correspond to approaching the van der Waals radii, which could influence the interlayer versus intralayer excitonic character, which would have an impact on how delocalized, and hence how tightly bound, the excitons are. The issue of interlayer versus intralayer character also plays a role in the peak in binding energy near 3 Å. From examining exciton densities (see description in Refs. [41,42]) we see that the maximum binding energy occurs just prior to a crossover from interlayer to intralayer excitons, in a region where the excitons are much more localized, resulting in large binding energies even with relatively small eigenvalues. For NiTTFtt, the pattern is more clear, where, generally, the binding energy peaks at low S-S distances where an interlayer exciton would be more localized and thus tightly bound and again peaks near the maximum eigenvalue. (Here we again focus on eigenvalues greater than ∼1.05.)

Previously, we observed system size to play an important role in the signature for condensation, which typically grows with system size in the materials we have explored. To understand the influence of system size on binding energy, we examine the binding energy in stacks of benzene and NiTTFtt with greater numbers of layers and extended chains in NiTTFtt. Figure 5 shows a plot of the binding energy and eigenvalues for increasingly large benzene stacks with 2.5 Å interlayer separation. Although the large eigenvalue signature increases almost linearly with the number of layers, the binding energy decreases as the system size grows. In the limit of a finite number of benzene layers the decrease appears

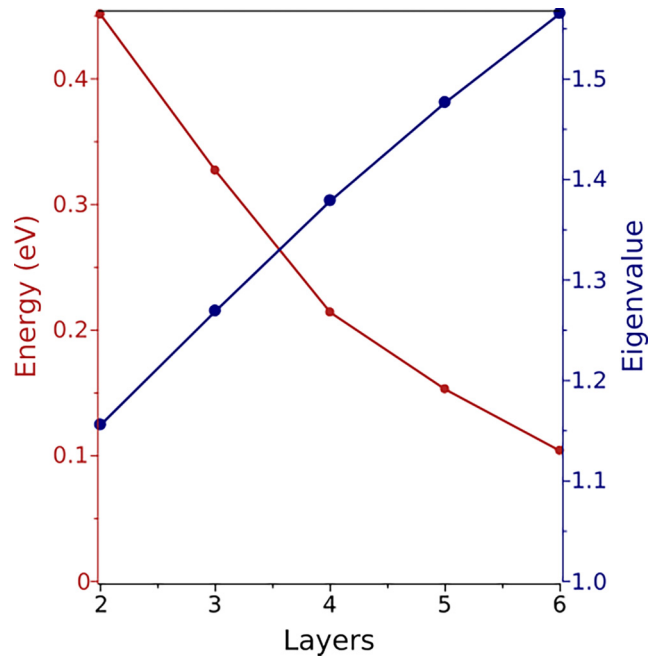

FIG. 5. The binding energies and eigenvalues versus the number of layers in a stack for stacks of benzene molecules.

to be continuous, but the flattening of the curve with larger numbers of layers suggests this behavior may be asymptotic, approaching a value in the large system limit that we would consider to be a "bulk material" binding energy. The trend is similar for NiTTFtt, decreasing from a binding energy of 78 meV for a bilayer to 25 meV for a stack of four NiTTFtt molecules. Horizontal growth also exhibits this trend, as a two-chain dimer with interlayer distance of 3.5 Å has a binding energy of ∼67 meV and a three-chain dimer has a binding energy of ∼32 meV, in spite of an increase in eigenvalue from 1.28 to 1.64. Such behavior is consistent with trends in binding energies calculated using other methods that show decreases in exciton binding energy with the number of layers in perovskites and the length of molecule for organic acenes [68–70], also appearing to approach a limit as the system size nears the bulk material. In our results, we hypothesize that the drop in binding energy in large systems results from increased exciton delocalization. Smaller systems have less space for exciton delocalization, forcing excitons closer together and enabling tighter binding, whereas in larger systems the excitons delocalize more and could be more loosely bound. This was evident from analyzing exciton densities (see Refs. [41,42]), where we observe increased delocalization of excitons in larger molecular stacks and chain lengths.

IV. DISCUSSION AND CONCLUSIONS

We presented a method for defining and calculating exciton binding energy rooted in the correlation associated with exciton condensation. The exciton binding energy is defined here as the energy required to remove an exciton from an exciton condensate. Using the large eigenvalue signature for exciton condensation, we calculated the binding energy as the difference between the ground state energy and a nonequilibrium

ground state energy for the same system, each state computed by semidefinite programming, with the nonequilibrium state subject to an additional constraint on the large eigenvalue. The relationship with exciton condensation ties this method for determining exciton binding energy inherently to correlation and the many-body nature of exciton condensation. Other approaches for calculating binding energy are generally based on mean-field references or orbital representations, and while correlation may be accounted for using the BSE and many-body perturbation theory, these approaches are strongly influenced by the reference calculation, usually done using density functional theory (DFT) [27]. Consequently, some of the limitations introduced by the DFT reference in treating strong correlation can be inherited by the results. This can introduce deficiencies in interpreting the interactions that are responsible for exciton formation and character in strongly correlated systems. Particularly for exciton condensation, which relies on strong correlation and many-body interactions to occur, methods based on a mean-field, single-particle picture that neglects many-body interactions may obscure the nature of excitons in an exciton condensate.

From our results for the Lipkin model, we observe that in the weakly interacting regime the traditional perspective of exciton binding agrees with the constrained definition, but the two diverge as the interaction and, consequently, the degree of condensation increase. In the weakly or noninteracting regime a mean-field perspective should be able to reasonably capture the character of an exciton, as in this case, but as the system moves into the highly interacting regime of exciton condensation, such a model will break down. As the two methods for calculating the binding energy diverge, the traditional picture of exciton binding is notably large, suggesting this result may correspond to overbinding. In a framework that accounts for some correlation, like the BSE, the difference would likely be smaller. However, overbinding has implications for prediction and characterization of exciton condensation, as predictions of the properties of exciton condensates, including the critical temperature, are often based on the magnitude of the exciton binding energy [7]. Using methods that predict artificially large exciton binding energies would lead to inaccurate characterization of the stability of an exciton condensate and overestimation of the critical temperature. Connecting exciton binding energy directly to condensation should better account for the interaction involved in exciton condensation and create a framework for characterizing excitonic properties in these systems.

Exciton condensation has been achieved in double-layer systems in which the electron and hole layers are separated and each is connected to a gate. In these types of devices, the carrier density is highly tunable via the bias voltage, allowing for control of the number of particles [33,34]. If the voltage were applied to a system exhibiting exciton condensation such that the number of excitons in the condensate changed from M to $M-1$, the difference in energy between the two could allow for experimental measurement of the exciton binding energy we describe.

Understanding the nature of excitons in exciton condensates is beneficial for predicting the formation of condensates and other properties like the critical temperature and density. Moreover, the nature of exciton binding in exciton condensates is associated with a crossover within the condensate state. Exciton condensation is understood to have two limits related to exciton binding: the BEC limit, where particles and holes are tightly bound and have high spatial localization, and the BCS limit, where particles and holes are loosely bound and spatially delocalized [71,72]. Through tuning of the interaction strengths and physical properties, exciton condensates shift from one limit to the other in a process known as BCS-BEC crossover. Because the two limits can be distinguished by the strength of binding and spatial localization, obtaining binding energy directly from a signature of exciton condensation that accounts for strong correlation could have important implications for exploring the BCS-BEC crossover.

ACKNOWLEDGMENTS

D.A.M. gratefully acknowledges the Department of Energy, Office of Basic Energy Sciences, Grant No. DE-SC0019215; U.S. National Science Foundation Grant No. CHE-2155082; and ACS Petroleum Research Fund Grant No. 61644-ND6. L.M.S.-S. acknowledges support from U.S. National Science Foundation Grant No. DGE-1746045.

APPENDIX

The energy is obtained using the variational 2-RDM (V2RDM) method [43–45,55–57], in which the energy is computed as a function of the 2-RDM according to the semidefinite program described in Eq. (6). In the V2RDM method, the constraint applies what are known as 2-positivity conditions so that

$$\begin{pmatrix} {}^2D & 0 & 0 \\ 0 & {}^2Q & 0 \\ 0 & 0 & {}^2G \end{pmatrix} \succeq 0, \tag{A1}$$

where ${}^2D$ is the 2-RDM [Eq. (3)], ${}^2Q$ is the two-hole RDM,

$${}^2Q^{j,k}_{l,i} = \langle \psi | \hat{a}_j \hat{a}_k \hat{a}_i^\dagger \hat{a}_l^\dagger | \psi \rangle, \tag{A2}$$

and ${}^2G$ is the particle-hole RDM [Eq. (1)]. Additionally, the 2-positivity conditions enforce linear mappings between pairs of the three two-body RDMs, ${}^2D$, ${}^2Q$, and ${}^2G$, as well as Hermiticity and antisymmetry requirements. An active space of size $[N, r]$, N particles in r orbitals, is treated with V2RDM, and the remaining orbitals are treated with a mean-field method. In the ground state calculation the active orbitals are optimized using the complete active space self-consistent-field method, and the same active orbitals are used for the nonequilibrium ground state calculation.

[1] F. London, On Bose-Einstein condensation, Phys. Rev. **54**, 947 (1938).

[2] J. Bardeen, L. N. Cooper, and J. R. Schrieffer, Theory of superconductivity, Phys. Rev. **108**, 1175 (1957).

[3] J. M. Blatt, K. W. Böer, and W. Brandt, Bose-Einstein condensation of excitons, Phys. Rev. **126**, 1691 (1962).

[4] O. Penrose and L. Onsager, Bose-Einstein condensation and liquid helium, Phys. Rev. **104**, 576 (1956).

[5] L. V. Keldysh, Coherent states of excitons, Phys. Usp. **60**, 1180 (2017).

[6] L. V. Butov, A. Zrenner, G. Abstreiter, G. Böhm, and G. Weimann, Condensation of indirect excitons in coupled AlAs/GaAs quantum wells, Phys. Rev. Lett. **73**, 304 (1994).

[7] M. M. Fogler, L. V. Butov, and K. S. Novoselov, High-temperature superfluidity with indirect excitons in van der Waals heterostructures, Nat. Commun. **5**, 4555 (2014).

[8] Z. Wang, D. A. Rhodes, K. Watanabe, T. Taniguchi, J. C. Hone, J. Shan, and K. F. Mak, Evidence of high-temperature exciton condensation in two-dimensional atomic double layers, Nature (London) **574**, 76 (2019).

[9] A. Kogar, M. S. Rak, S. Vig, A. A. Husain, F. Flicker, Y. I. Joe, L. Venema, G. J. MacDougall, T. C. Chiang, E. Fradkin, J. van Wezel, and P. Abbamonte, Signatures of exciton condensation in a transition metal dichalcogenide, Science **358**, 1314 (2017).

[10] D. Wang, N. Luo, W. Duan, and X. Zou, High-temperature excitonic Bose–Einstein condensate in centrosymmetric two-dimensional semiconductors, J. Phys. Chem. Lett. **12**, 5479 (2021).

[11] K. Ulman and S. Y. Quek, Organic-2D material heterostructures: A promising platform for exciton condensation and multiplication, Nano Lett. **21**, 8888 (2021).

[12] L. Sigl, F. Sigger, F. Kronowetter, J. Kiemle, J. Klein, K. Watanabe, T. Taniguchi, J. J. Finley, U. Wurstbauer, and A. W. Holleitner, Signatures of a degenerate many-body state of interlayer excitons in a van der Waals heterostack, Phys. Rev. Res. **2**, 042044(R) (2020).

[13] M. S. Fuhrer and A. R. Hamilton, Chasing the exciton condensate, Phyics **9**, 80 (2016).

[14] J. J. Su and A. H. MacDonald, Spatially indirect exciton condensate phases in double bilayer graphene, Phys. Rev. B **95**, 045416 (2017).

[15] X. Liu, K. Watanabe, T. Taniguchi, B. I. Halperin, and P. Kim, Quantum Hall drag of exciton condensate in graphene, Nat. Phys. **13**, 746 (2017).

[16] S. Pannir-Sivajothi, J. A. Campos-Gonzalez-Angulo, L. A. Martínez-Martínez, S. Sinha, and J. Yuen-Zhou, Driving chemical reactions with polariton condensates, Nat. Commun. **13**, 1645 (2022).

[17] D. Jérome, T. M. Rice, and W. Kohn, Excitonic insulator, Phys. Rev. **158**, 462 (1967).

[18] L. Du, X. Li, W. Lou, G. Sullivan, K. Chang, J. Kono, and R.-R. Du, Evidence for a topological excitonic insulator in InAs/GaSb bilayers, Nat. Commun. **8**, 1971 (2017).

[19] Y. Jia *et al.*, Evidence for a monolayer excitonic insulator, Nat. Phys. **18**, 87 (2022).

[20] G. H. Wannier, The structure of electronic excitation levels in insulating crystals, Phys. Rev. **52**, 191 (1937).

[21] T. Olsen, S. Latini, F. Rasmussen, and K. S. Thygesen, Simple screened hydrogen model of excitons in two-dimensional materials, Phys. Rev. Lett. **116**, 056401 (2016).

[22] V. Turkowski, A. Leonardo, and C. A. Ullrich, Time-dependent density-functional approach for exciton binding energies, Phys. Rev. B **79**, 233201 (2009).

[23] C. Klingshirn, Excitons, biexcitons and trions, *Semiconductor Optics* (Springer, Berlin, 2007), pp. 243–264

[24] J.-L. Bredas, Mind the gap! Mater. Horiz. **1**, 17 (2014).

[25] M. Rohlfing and S. G. Louie, Electron-hole excitations and optical spectra from first principles, Phys. Rev. B **62**, 4927 (2000).

[26] G. Onida, L. Reining, and A. Rubio, Electronic excitations: Density-functional versus many-body Green's-function approaches, Rev. Mod. Phys. **74**, 601 (2002).

[27] X. Blase, I. Duchemin, D. Jacquemin, and P.-F. Loos, The Bethe–Salpeter equation formalism: From physics to chemistry, J. Phys. Chem. Lett. **11**, 7371 (2020).

[28] D. Varsano, M. Palummo, E. Molinari, and M. Rontani, A monolayer transition-metal dichalcogenide as a topological excitonic insulator, Nat. Nanotechnol. **15**, 367 (2020).

[29] S. S. Ataei, D. Varsano, E. Molinari, and M. Rontani, Evidence of ideal excitonic insulator in bulk MoS_2 under pressure, Proc. Natl. Acad. Sci. USA **118**, e2010110118 (2021).

[30] M. M. Quintela, A. Costa, and N. Peres, Excitonic instability in transition metal dichalcogenides, J. Phys.: Condens. Matter **34**, 455303 (2022).

[31] Q. He, X. Que, L. Zhou, M. Isobe, D. Huang, and H. Takagi, Tunneling-tip-induced collapse of the charge gap in the excitonic insulator Ta_2NiSe_5, Phys. Rev. Res. **3**, L032074 (2021).

[32] P. B. Littlewood and X. Zhu, Possibilities for exciton condensation in semiconductor quantum-well structures, Phys. Scr. **T68**, 56 (1996).

[33] B. Sun, W. Zhao, T. Palomaki, Z. Fei, E. Runburg, P. Malinowski, X. Huang, J. Cenker, Y.-T. Cui, J.-H. Chu, X. Xu, S. S. Ataei, D. Varsano, M. Palummo, E. Molinari, M. Rontani, and D. H. Cobden, Evidence for equilibrium exciton condensation in monolayer WTe_2, Nat. Phys. **18**, 94 (2022).

[34] L. Ma, P. X. Nguyen, Z. Wang, Y. Zeng, K. Watanabe, T. Taniguchi, A. H. MacDonald, K. F. Mak, and J. Shan, Strongly correlated excitonic insulator in atomic double layers, Nature (London) **598**, 585 (2021).

[35] Y. Zeng and A. H. MacDonald, Electrically controlled two-dimensional electron-hole fluids, Phys. Rev. B **102**, 085154 (2020).

[36] R. Qi, A. Y. Joe, Z. Zhang, Y. Zeng, T. Zheng, Q. Feng, J. Xie, E. Regan, Z. Lu, T. Taniguchi, K. Watanabe, S. Tongay, M. F. Crommie, A. H. MacDonald, and F. Wang, Thermodynamic behavior of correlated electron-hole fluids in van der Waals heterostructures, Nat. Commun. **14**, 8264 (2023).

[37] S. De Palo, P. E. Trevisanutto, G. Senatore, and G. Vignale, Collective excitations and quantum incompressibility in electron-hole bilayers, Phys. Rev. B **104**, 115165 (2021).

[38] C. Garrod and M. Rosina, Particle-hole matrix: Its connection with the symmetries and collective features of the ground state, J. Math. Phys. **10**, 1855 (1969).

[39] S. Safaei and D. A. Mazziotti, Quantum signature of exciton condensation, Phys. Rev. B **98**, 045122 (2018).

[40] H. Lipkin, N. Meshkov, and A. Glick, Validity of many-body approximation methods for a solvable model: (I). Exact solutions and perturbation theory, Nucl. Phys. **62**, 188 (1965).

[41] A. O. Schouten, L. M. Sager, and D. A. Mazziotti, Exciton condensation in molecular-scale van der Waals stacks, J. Phys. Chem. Lett. **12**, 9906 (2021).

[42] A. O. Schouten, J. E. Klevens, L. M. Sager-Smith, J. Xie, J. S. Anderson, and D. A. Mazziotti, Potential for exciton condensation in a highly conductive amorphous polymer, Phys. Rev. Mater. **7**, 045001 (2023).

[43] D. A. Mazziotti, Two-electron reduced density matrix as the basic variable in many-electron quantum chemistry and physics, Chem. Rev. **112**, 244 (2012).

[44] D. A. Mazziotti, *Reduced-Density-Matrix Mechanics: With Application to Many-Electron Atoms and Molecule*, Advances in Chemical Physics Vol. 134 (Wiley, New York, 2007).

[45] D. A. Mazziotti, Large-scale semidefinite programming for many-electron quantum mechanics, Phys. Rev. Lett. **106**, 083001 (2011).

[46] J.-N. Boyn, J. Xie, J. S. Anderson, and D. A. Mazziotti, Entangled electrons drive a non-superexchange mechanism in a cobalt quinoid dimer complex, J. Phys. Chem. Lett. **11**, 4584 (2020).

[47] S. Ewing and D. A. Mazziotti, Correlation-driven phenomena in periodic molecular systems from variational two-electron reduced density matrix theory, J. Chem. Phys. **154**, 214106 (2021).

[48] A. W. Schlimgen, C. W. Heaps, and D. A. Mazziotti, Entangled electrons foil synthesis of elusive low-valent vanadium oxo complex, J. Phys. Chem. Lett. **7**, 627 (2016).

[49] J. Xie, S. Ewing, J.-N. Boyn, A. S. Filatov, B. Cheng, T. Ma, G. L. Grocke, N. Zhao, R. Itani, X. Sun, H. Cho, Z. Chen, K. W. Chapman, S. N. Patel, D. V. Talapin, J. Park, D. A. Mazziotti, and J. S. Anderson, Intrinsic glassy-metallic transport in an amorphous coordination polymer, Nature (London) **611**, 479 (2022).

[50] C. N. Yang, Concept of off-diagonal long-range order and the quantum phases of liquid He and of superconductors, Rev. Mod. Phys. **34**, 694 (1962).

[51] F. Sasaki, Eigenvalues of fermion density matrices, Phys. Rev. **138**, B1338 (1965).

[52] A. J. Coleman, Structure of fermion density matrices, Rev. Mod. Phys. **35**, 668 (1963).

[53] D. A. Mazziotti and R. M. Erdahl, Uncertainty relations and reduced density matrices: Mapping many-body quantum mechanics onto four particles, Phys. Rev. A **63**, 042113 (2001).

[54] D. A. Mazziotti, Structure of fermionic density matrices: Complete N-representability conditions, Phys. Rev. Lett. **108**, 263002 (2012).

[55] D. A. Mazziotti, Realization of quantum chemistry without wave functions through first-order semidefinite programming, Phys. Rev. Lett. **93**, 213001 (2004).

[56] M. Fukuda, B. J. Braams, M. Nakata, M. L. Overton, J. K. Percus, M. Yamashita, and Z. Zhao, Large-scale semidefinite programs in electronic structure calculation, Math. Program. **109**, 553 (2007).

[57] D. A. Mazziotti, Quantum many-body theory from a solution of the N-representability problem, Phys. Rev. Lett. **130**, 153001 (2023).

[58] L. M. Sager and D. A. Mazziotti, Simultaneous fermion and exciton condensations from a model Hamiltonian, Phys. Rev. B **105**, 035143 (2022).

[59] *Quantum Chemistry Toolbox in Maple* (RDMChem, Chicago, 2024).

[60] *Maple* (Maplesoft, Waterloo, Ontario, 2024).

[61] C. Cocchi and C. Draxl, Optical spectra from molecules to crystals: Insight from many-body perturbation theory, Phys. Rev. B **92**, 205126 (2015).

[62] D. Hirose, Y. Noguchi, and O. Sugino, All-electron GW+Bethe-Salpeter calculations on small molecules, Phys. Rev. B **91**, 205111 (2015).

[63] J. Sworakowski, How accurate are energies of HOMO and LUMO levels in small-molecule organic semiconductors determined from cyclic voltammetry or optical spectroscopy? Synth. Met. **235**, 125 (2018).

[64] P. K. Nayak, Exciton binding energy in small organic conjugated molecule, Synth. Met. **174**, 42 (2013).

[65] I. Hill, A. Kahn, Z. Soos, and R. Pascal, Jr., Charge-separation energy in films of π-conjugated organic molecules, Chem. Phys. Lett. **327**, 181 (2000).

[66] M. Dvorak, S.-H. Wei, and Z. Wu, Origin of the variation of exciton binding energy in semiconductors, Phys. Rev. Lett. **110**, 016402 (2013).

[67] J. P. Eisenstein and A. H. MacDonald, Bose-Einstein condensation of excitons in bilayer electron systems, Nature (London) **432**, 691 (2004).

[68] Y. Cho and T. C. Berkelbach, Optical properties of layered hybrid organic–inorganic halide perovskites: A tight-binding GW-BSE study, J. Phys. Chem. Lett. **10**, 6189 (2019).

[69] K. Hummer and C. Ambrosch-Draxl, Oligoacene exciton binding energies: Their dependence on molecular size, Phys. Rev. B **71**, 081202(R) (2005).

[70] M. Knupfer, Exciton binding energies in organic semiconductors, Appl. Phys. A **77**, 623 (2003).

[71] A. J. Leggett and S. Zhang, The BEC–BCS crossover: Some history and some general observations, in *The BCS-BEC Crossover and the Unitary Fermi Gas*, edited by W. Zwerger (Springer, Berlin, 2012), pp. 33–47.

[72] M. Randeria and E. Taylor, Crossover from Bardeen-Cooper-Schrieffer to Bose-Einstein condensation and the unitary fermi gas, Annu. Rev. Condens. Matter Phys. **5**, 209 (2014).